

Momentum-dependent hybridization gap and dispersive in-gap state of the Kondo semiconductor SmB_6

Hidetoshi Miyazaki,^{1,*} Tetsuya Hajiri,^{1,2} Takahiro Ito,² Satoru Kunii,³ and Shin-ichi Kimura^{1,4,†}

¹*UVSOR Facility, Institute for Molecular Science, Okazaki 444-8585, Japan*

²*Graduate School of Engineering, Nagoya University, Nagoya 464-8603, Japan*

³*Department of Physics, Tohoku University, Sendai 980-8578, Japan*

⁴*School of Physical Sciences, The Graduate University for Advanced Studies (SOKENDAI), Okazaki 444-8585, Japan*

(Received 15 June 2011; revised manuscript received 15 March 2012; published 6 August 2012)

We report the temperature-dependent three-dimensional angle-resolved photoemission spectra of the Kondo semiconductor SmB_6 . We found a difference in the temperature dependence of the peaks at the X and Γ points, due to hybridization between the $\text{Sm } 5d$ conduction band and the nearly localized $\text{Sm } 4f$ state. The peak intensity at the X point has the same temperature dependence as the valence transition below 120 K, while that at the Γ point is consistent with the magnetic excitation at $Q = (0.5, 0.5, 0.5)$ below 30 K. This suggests that the hybridization with the valence transition mainly occurs near the X point, and the initial state of the magnetic excitation is located near the Γ point.

DOI: [10.1103/PhysRevB.86.075105](https://doi.org/10.1103/PhysRevB.86.075105)

PACS number(s): 71.27.+a, 79.60.-i

Materials with strong electron correlation have exotic physical properties that cannot be predicted from first-principle band calculations. One example may be seen in a semiconductor with a very small energy gap, which appears in rare-earth compounds such as the Kondo semiconductor or insulator (KI).¹ At high temperatures, KI behaves as a dense Kondo metal, while an energy gap with an activation energy of several 10 meV appears at low temperature. The energy gap is believed to originate from hybridization between the nearly localized $4f$ state near the Fermi level (E_F) and the conduction band (c - f hybridization).

Numerous studies have investigated the energy gap of KI, using optical conductivity,^{2,3} point-contact spectroscopy,⁴ angle-integrated photoemission spectroscopy,^{5,6} and other methods. However, the momentum dependence of the c - f hybridization gap, as well as the relation of the electronic structure to other physical properties, needs to be studied. Because the c - f hybridization occurs at a specific momentum vector, the most direct method of observing the band dispersion of the c - f hybridization gap is three-dimensional angle-resolved photoemission spectroscopy (3D-ARPES) using a tunable photon source from synchrotron radiation. Thus, we applied the 3D-ARPES method to observe the c - f hybridization gap creation of a typical KI, SmB_6 .

SmB_6 is a valence-fluctuation material in between $\text{Sm}^{2+}(4f^6)$ and $\text{Sm}^{3+}(4f^5)$ ions.⁷ The electrical resistivity (ρ) decreases on cooling, as a metal, above a temperature of 100 K, but then reveals a semiconductorlike character with an activation energy of 15 meV.⁸ There are two characteristic temperatures on SmB_6 ; one is the valence transition below 120 K, and the other is magnetic excitation below 30 K. The mean valence changes from 2.57 at 120 K to 2.50 at 40 K on cooling.⁹ Coincidentally, the lattice constant, which normally shrinks above 120 K on cooling, anomalously expands from 120 K to a few tens K, indicating the valence change from Sm^{3+} to Sm^{2+} .¹⁰ On the other hand, the magnetic excitation at the scattering vector of $Q = (0.5, 0.5, 0.5)$, observed by inelastic neutron scattering (INS), rapidly increases below 30 K.¹¹ Then the mean valence slightly recovers from 2.50 to 2.52

below 30 K, and the lattice constant shrinks again. The reason for the different temperature dependence between the magnetic excitation and the valence transition needs to be determined. At temperatures lower than 10 K, another gap (in-gap state) has been noted at about 4 meV through the observations of optical conductivity,^{3,12} point-contact spectroscopy,⁴ and angle-integrated photoemission spectroscopy.⁵ Below 3 K, ρ becomes saturated and has a residual resistivity of several Ω cm.¹³ Recently, the residual resistivity has been suggested to originate from metallic behavior at the edge state on the surface [topological KI (TKI)]¹⁴ and other reasons, but the relation of the electronic state to the in-gap state, needs to be investigated experimentally.

In this paper, we report the temperature dependence of the dispersion curve of the hybridization state using temperature-dependent 3D-ARPES, in order to determine the electronic structure and the reason for the different temperature dependences of the valence transition and magnetic excitation. We found that the hybridization band with a peak at a binding energy (E_B) of 15 meV near the X point gradually appears on cooling from 150 to 40 K, which has the same temperature dependence as the valence transition. At the Γ point, on the other hand, the peak at $E_B \sim 20$ meV has the same temperature dependence as the magnetic excitation at $Q = (0.5, 0.5, 0.5)$, which differs from the 15-meV peak at the X point. This suggests that the magnetic excitation originates from the hybridization band at the Γ point.

A high purity single crystal of SmB_6 was grown by the floating-zone method.¹⁵ The sample cut along the (001) plane was cleaned by argon sputtering and annealing at 1400 °C, by using an infrared heating system under a vacuum of 10^{-8} Pa. The low-energy electron diffraction (LEED) image of the clean surface is shown in Fig. 1(a). The LEED image indicates that the SmB_6 (001) surface has not only 1×1 of the bulk but also a superlattice structure of 2×1 of the surface, which is similar to a previous result.¹⁶

Since the peak intensity of the 2×1 diffraction is about half that of the 1×1 diffraction and the background is not higher than the previous result, the well-defined surface state

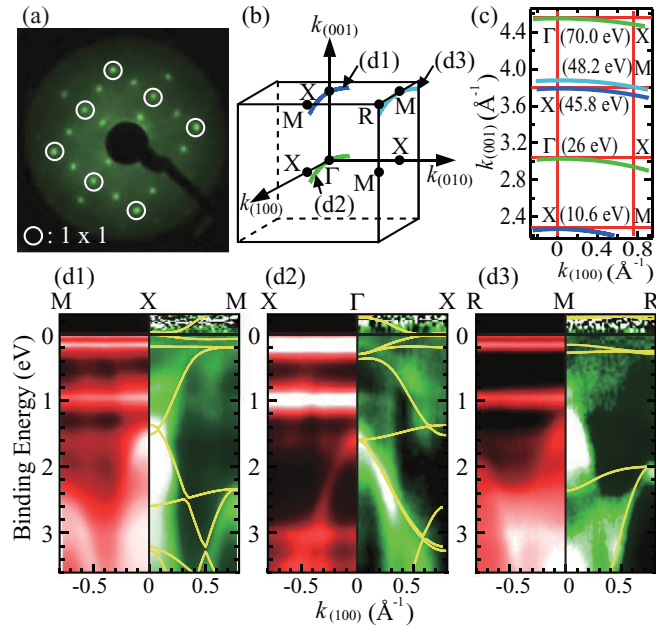


FIG. 1. (Color online) (a) Low-energy electron diffraction (LEED) pattern of the SmB₆ (001) surface with an electron energy of 100 eV. Spots marked by circles represent diffractions of 1 × 1; other spots represent 1 × 2 and higher order diffractions. (b) The first Brillouin zone of SmB₆ and high-symmetry points. (c) The photon energies corresponding to the Γ and X points in normal emission geometry and the M point in grazing emission geometry. (d1)–(d3) ARPES intensity mapping images and calculated band dispersions (solid lines) on the M-X ($h\nu = 45.8$ eV), X-Γ (70.0 eV), and R-M (48.2 eV) lines at 10 K. The left-hand images in each panel are the ARPES intensity mappings, which emphasize flat bands, and the right-hand images are the same intensity mappings but divided by angle-integrated photoemission spectra, which emphasize highly dispersive bands.

was obtained. However, the surface state is mostly boron-terminated B₆; i.e., the Sm atoms do not appear as much on the surface. Therefore the surface state derived from Sm is expected to be suppressed.

Normal-emission and in-plane ARPES experiments in the vacuum-ultraviolet region were performed at beamlines 5U (Ref. 17) and 7U,¹⁸ respectively, of the UVSOR-II storage ring, Institute for Molecular Science. The photon energies corresponding to high-symmetry k_z points, as shown in Fig. 1(b) were determined by using normal emission ARPES taken at BL5U [Fig. 1(c)]. The inner potential was determined as 13.5 eV. Using the obtained high-symmetry points, the temperature dependence of high-resolution ARPES spectra at the Γ and X points was measured at BL7U. The total energy resolutions were about 50 meV at BL5U and 5 meV at BL7U, and the vacuum during the measurement was less than 5×10^{-9} Pa. A local density approximation (LDA) band structure calculation was performed by the full potential linearized augmented plane wave plus local orbital (LAPW + lo) method including spin-orbit coupling implemented in the WIEN2K code.¹⁹

Figures 1(d1)–1(d3) are the ARPES images of the M-X, X-Γ, and R-M lines, taken at photon energies of 45.8, 70.0, and 48.2 eV, respectively, and the corresponding band calculation results. The photon energies at the high-symmetry points are

consistent with a previous work.²⁰ The flat bands at the binding energies (E_B) of 0, 0.2, 1, and 3 eV can be recognized as the multiplet structures of ${}^6H_{5/2}$, ${}^6H_{7/2}$, 6F , and 6P of the Sm²⁺ final state, respectively. There is another flat band at $E_B \sim 1.5$ eV, which seems to originate from the surface state of Sm 4*f*, but the intensity is not great, because the surface is terminated by boron atoms. The highly dispersive valence bands at $E_B \geq 1.4$ eV and the conduction band at $E_B \leq 1.5$ eV at the X point originate from the *sp* covalent state of the B₆ network and the Sm 5*d* state, respectively. These higher- E_B bands are in good agreement with the band structure calculation with a holelike band appearing at $E_B \geq 1$ eV owing to k_z broadening. The intensities of the Sm²⁺ final-state multiplet 6H and 6F are greater near the X point than those at the M point. This implies that the hybridization occurs near the X point. The band calculation in the right-hand images of Figs. 1(d1) and 1(d2) also indicated that the hybridization gap opens near the X point. It should be noted that, however, the band calculation has much overstated Sm 4*f* bandwidths and hybridization effects, the failure to describe the mixed valency, and lack of final-state multiplet structure.

To investigate the *c-f* hybridization gap formation, we measured the temperature dependence of the Sm 5*d* character of the hybridization gap (peak) in energy distribution curves (EDCs) at the X and Γ points, as shown in Fig. 2. Because of the hybridization between the Sm 5*d* and 4*f* states, the 4*f* feature must appear in the Sm 5*d* EDC. Then we used low photon energies of 10.6 eV for the X point and 26 eV for the Γ point, because the Sm 4*f* cross section can be strongly suppressed by using lower energy photons below 30 eV.²¹ The temperature dependence of EDCs obtained at the X and Γ points is shown in Figs. 2(a1) and 2(a2). At 10 K, there are peaks at $E_B \sim 15$ meV at the X point, and at 20 meV at the Γ point. These peaks have different temperature dependences. Figures 2(b1) and (b2) are the same spectra as in Figs. 2(a1) and 2(a2), respectively, divided by the Fermi-Dirac distribution curve. Clear energy gaps appear above E_F at both the X and Γ points. Because the EDCs originate from the Sm 5*d* states, the peaks at the gap edges are evidence of the hybridization with the Sm 4*f* states. At the X point, the peak becomes visible at 100 K and increases on cooling. To clarify the relation of these peaks to other physical properties, the temperature dependence of the peak is plotted in Fig. 2(c1). The peak intensity gradually increases below 150 K. The temperature dependence of the peak is very similar to the valence transition (2.57 at 120 K → 2.50 at 40 K) observed by using x-ray absorption spectroscopy at the Sm *L*₃ edge, as shown in Fig. 2(c1).⁹ Therefore the temperature dependence of the 15-meV peak at the X point indicates the change in the hybridization intensity, i.e., the hybridization gap opens near the X point. This is roughly consistent with the LDA band calculation as shown in Fig. 1, in which the hybridization between the Sm 5*d* conduction band and 4*f*_{5/2} states appears near the X point, but the experimental 4*f* bandwidth is much smaller than that in the calculation. The discussion is done later. On cooling, the hybridization becomes stable, and the mean valence shifts to divalent.

At the Γ point, on the other hand, the temperature dependence of the 18-meV peak is not the same as the 15-meV peak at the X point. The spectrum in Fig. 2(b2) has no energy gap above 80 K. However, the energy gap with the 18-meV peak

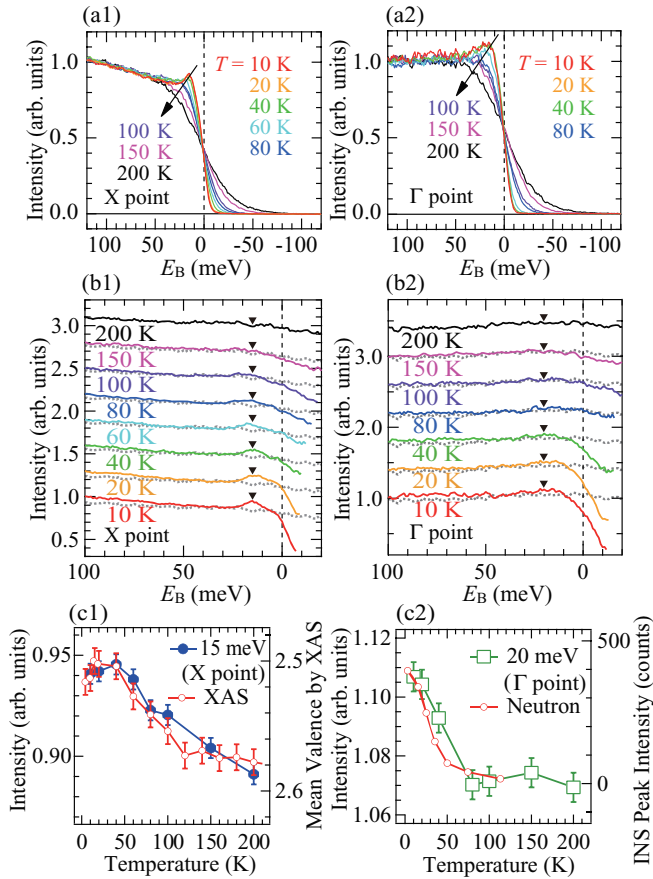


FIG. 2. (Color online) Temperature dependence of energy distribution curves (EDCs) at the X point [$h\nu = 10.6$ eV (a1)] and the Γ point [26 eV (a2)], and their spectra divided by the Fermi-Dirac distribution curve [(b1), (b2)]. EDCs were normalized at the binding energy E_B of 120 meV. Successive curves in (b1) and (b2) are offset by 0.3 and 0.4 , respectively, for clarity. The dotted lines in (b1) and (b2) are the spectra at 200 K. The temperature-dependent peak intensities relative to the intensity at 200 K of the 15 -meV peak at the X point (c1) and of the 20 -meV peak at the Γ point (c2). The mean valence number evaluated by the x-ray absorption spectroscopy (XAS) (Ref. 9) and the peak intensity of the inelastic neutron scattering (INS) at $Q = (0.5, 0.5, 0.5)$ (Ref. 11) are also plotted.

rapidly appears below 40 K, which differs from the temperature dependence of the 15 -meV peak at the X point. In Fig. 2(c2), the temperature dependence of the relative intensity of the 18 -meV peak is plotted, and its peak intensity has the same temperature dependence as the magnetic excitation at $Q = (0.5, 0.5, 0.5)$ by INS.¹¹ The temperature dependence of the 18 -meV peak is consistent with that of the magnetic excitation, suggesting that the 18 -meV peak at the Γ point (i.e., the hybridization band at the Γ point) is the initial state of the magnetic excitation. The appearance of the charge and spin excitations at different k points is consistent with a mean-field theory based on the periodic Anderson model²² and with the assumption of the spin exciton theory.²³ Strictly speaking, however, the peak energies of the magnetic excitations observed by INS and the Raman scattering²⁴ are about 14 and 16 meV, respectively, which is slightly lower energy than the 18 -meV EDC peak. This might

indicate the property of the spin exciton²³ or there might be magnetic excitations at higher energy region similar to that of other KI, YbB₁₂.²⁵

In the spin-polarized local-density approximation (LSDA) + U band calculation with Sm³⁺ ions,²⁶ the energy level of the Sm³⁺ $5d$ state is close to that of the $4f_{7/2}$ state near the Γ point. Then the hybridization between these states would occur at the Γ point. Due to the opposite logic of the hybridization in the Sm²⁺ ions at the X point, the hybridization in the Sm³⁺ ions means that the mean valence shifts to trivalent. This is consistent with the evidence of the increase in the mean valence below 30 K.⁹

The creation of the hybridization gap is here described in detail. The temperature-dependent ARPES spectra, divided by the Fermi-Dirac distribution curve along the X-M line, are plotted in Fig. 3(a). At $T = 40$ K in Fig. 3(a), the k dependence of the peak at $E_B = 15$ meV is almost flat. The band becomes dispersive below 20 K, as shown in Fig. 3(b). At 10 K, the band dispersion is very similar to that of the LDA band calculation, but the energy of the peak at $k_{(100)} = 0.4 \text{ \AA}^{-1}$ is about 18 meV, which is much lower than the calculated result of 70 meV. The width of the experimental $4f$ band dispersion is about 3 meV, which is also much smaller than that of the calculation (~ 50 meV). This suggests that

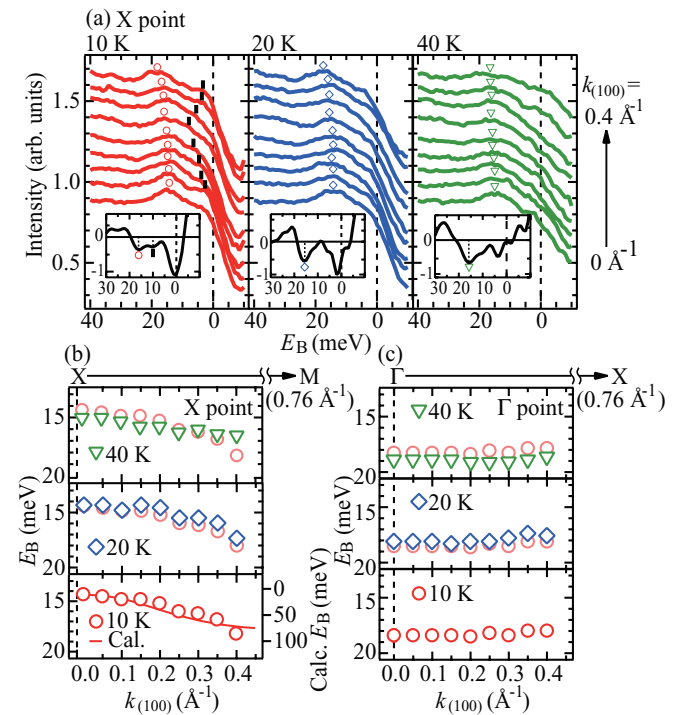


FIG. 3. (Color online) (a) Temperature dependence of energy distribution curves (EDCs) divided by the Fermi-Dirac distribution curve in the X (0 \AA^{-1})-M (0.76 \AA^{-1}) line, using 10.6 -eV photon energy. The hybridization band dispersions are shown by open circles, and the observed dispersive in-gap state is shown by vertical lines. Insets show the second derivative curves of smoothed EDCs at $k_{(100)} = 0.25 \text{ \AA}^{-1}$. The marks correspond to the band dispersions. Temperature dependence of the hybridization band in the X-M line [$h\nu = 10.6$ eV (b)] and the Γ -X line [$h\nu = 26.0$ eV (c)]. The band dispersion derived from the LDA calculation [Fig. 1(d1)] with the energy scale in the right axis is also plotted by a solid line in (b).

the $4f$ band is strongly renormalized by the strong electron correlation. Note that the band dispersion near the Γ point shown in Fig. 3(c) is almost flat, and is also located at much lower energy than that in the LDA calculation ($E_B \sim 0.3$ eV), as shown in Fig. 1(d2), indicating a stronger localization at the Γ point than that at the X point. This is consistent with the argument in Fig. 2; i.e., the hybridization gap opens near the X point, while the initial state of the magnetic excitation is the Γ point. The peak energy at the X point is about 15 meV, which is roughly consistent with the valence transition temperature of 120 K (~ 10 meV). However, the peak energy of 20 meV at the Γ point is much higher energy than the appearance temperature of the magnetic excitation (50 K ~ 4 meV). This also suggests that the magnetic excitation is strongly correlated.

At $T = 10$ K, another band dispersion, with an electronlike dispersion at $k \sim 0.25 \text{ \AA}^{-1}$ and a holelike one at $k \sim 0 \text{ \AA}^{-1}$, seems to appear at $E_B \sim 8$ meV, as shown by vertical lines in Fig. 3(a). The dispersion curve of the in-gap state is very

similar to the strong coupled TKI.^{27,28} A detailed discussion will be presented in a separate paper.²⁹

To summarize, we have investigated the momentum-dependent hybridization state between the conduction band and $4f$ states of SmB_6 by using a three-dimensional angle-resolved photoemission spectroscopy. The temperature dependence of the energy distribution curves suggests that the hybridization state at the binding energy of 15 meV near the X point is the origin of the valence transition below 120 K, while that at 20 meV at the Γ point is the initial state of the magnetic excitation at $Q = (0.5, 0.5, 0.5)$ with strong electron correlation.

We would like to thank M. Dzero, P. Coleman, and M. Matsunami for their fruitful discussion. Part of this work was performed by the Use-of-UVSOR Facility Program of the Institute for Molecular Science. The work was partly supported by a Grant-in-Aid for Scientific Research (B) from JSPS of Japan (Grant No. 22340107).

*Present address: Center for Fostering Young and Innovative Researchers, Nagoya Institute of Technology, Nagoya 466-8555, Japan.

†kimura@ims.ac.jp

¹G. Aeppli and Z. Fisk, *Comments Condens. Matter Phys.* **16**, 155 (1992), and references therein.

²G. Travaglini and P. Wachter, *Phys. Rev. B* **29**, 893 (1984).

³S. I. Kimura, T. Nanba, S. Kunii, and T. Kasuya, *Phys. Rev. B* **50**, 1406 (1994).

⁴K. Flachbart, K. Gloos, E. Konovalova, Y. Paderno, M. Reiffers, P. Samuely, and P. Švec, *Phys. Rev. B* **64**, 085104 (2001).

⁵S. Nozawa, T. Tsukamoto, K. Kawai, T. Haruna, S. Shin, and S. Kunii, *J. Phys. Chem. Solids* **63**, 1223 (2002).

⁶S. Souma, H. Kumigashira, T. Ito, T. Takahashi, and S. Kunii, *Physica B* **312–313**, 329 (2002).

⁷R. L. Cohen, M. Eibschütz, K. W. West, and E. Buehler, *J. Appl. Phys.* **41**, 898 (1970).

⁸T. Tanaka, R. Nishitani, C. Oshima, E. Bannai, and S. Kawai, *J. Appl. Phys.* **51**, 3877 (1980).

⁹M. Mizumaki, S. Tsutsui, and F. Iga, *J. Phys.: Conf. Ser.* **176**, 012034 (2009).

¹⁰T. Kasuya, K. Takegahara, Y. Aoki, K. Hanzawa, M. Kasaya, S. Kunii, T. Fujita, N. Sato, H. Kimura, T. Komatsubara, T. Furuno, and J. Rossat-Mignod, in *Valence Fluctuations in Solids*, edited by L. M. Falicov, W. Hanke, and M. B. Maple (North-Holland, Amsterdam, 1981), p. 215.

¹¹P. A. Alekseev, J.-M. Mignot, J. Rossat-Mignod, V. N. Lazukov, I. P. Sadikov, E. S. Konovalova, and Yu. B. Paderno, *J. Phys.: Condens. Matter* **7**, 289 (1995).

¹²B. Gorshunov, N. Sluchanko, A. Volkov, M. Dressel, G. Knebel, A. Loidl, and S. Kunii, *Phys. Rev. B* **59**, 1808 (1999).

¹³J. C. Cooley, M. C. Aronson, Z. Fisk, and P. C. Canfield, *Phys. Rev. Lett.* **74**, 1629 (1995).

¹⁴M. Dzero, K. Sun, V. Galitski, and P. Coleman, *Phys. Rev. Lett.* **104**, 106408 (2010).

¹⁵T. Tanaka, E. Bannai, S. Kawai, and T. Yamane, *J. Cryst. Growth* **30**, 193 (1975).

¹⁶M. Aono, R. Nishitani, T. Tanaka, E. Bannai, and S. Kawai, *Solid State Commun.* **28**, 409 (1978).

¹⁷T. Ito, S. Kimura, H. J. Im, E. Nakamura, M. Sakai, T. Horigome, K. Soda, and T. Takeuchi, in *Proceedings of the Ninth International Conference on Synchrotron Radiation Instrumentation*, edited by J.-Y. Choi and S. Rah, *AIP Conf. Proc. No. 879* (AIP, Melville, NY, 2007), p. 587.

¹⁸S. Kimura, T. Ito, M. Sakai, E. Nakamura, N. Kondo, K. Hayashi, T. Horigome, M. Hosaka, M. Katoh, T. Goto, T. Ejima, and K. Soda, *Rev. Sci. Instrum.* **81**, 053104 (2010).

¹⁹P. Blaha, K. Schwarz, P. Sorantin, and S. B. Trickey, *Comput. Phys. Commun.* **59**, 399 (1990).

²⁰J. D. Denlinger, G.-H. Gweon, J. W. Allen, C. G. Olson, Y. Dalichaouch, B.-W. Lee, M. B. Maple, Z. Fisk, P. C. Canfield, and P. E. Armstrong, *Physica B* **281–282**, 716 (2000).

²¹J. J. Yeh and I. Lindau, *At. Data Nucl. Data Tables* **32**, 1 (1985).

²²P. S. Riseborough, *Phys. Rev. B* **45**, 13984 (1992).

²³A. Akbari, P. Thalmeier, and P. Fulde, *Phys. Rev. Lett.* **102**, 106402 (2009).

²⁴P. Nyhus, S. L. Cooper, Z. Fisk, and J. Sarrao, *Phys. Rev. B* **55**, 12488 (1997).

²⁵K. S. Nemkovski, J.-M. Mignot, P. A. Alekseev, A. S. Ivanov, E. V. Nefedova, A. V. Rybina, L.-P. Regnault, F. Iga, and T. Takabatake, *Phys. Rev. Lett.* **99**, 137204 (2007).

²⁶V. N. Antonov, B. N. Harmon, and A. N. Yaresko, *Phys. Rev. B* **66**, 165209 (2002).

²⁷T. Takimoto, *J. Phys. Soc. Jpn.* **80**, 123710 (2011).

²⁸M. Dzero, K. Sun, P. Coleman, and V. Galitski, *Phys. Rev. B* **85**, 045130 (2012).

²⁹S. Kimura, T. Hajiri, M. Matsunami, H. Miyazaki, and S. Kumii (unpublished).